Geol. Mag. **149** (*5*), *2012, pp. 783–797.* © *Cambridge University Press 2011*
doi:10.1017/S0016756811000975

U–Pb zircon dating and Sr–Nd–Hf isotopic evidence to support a juvenile origin of the ∼ 634 Ma El Shalul granitic gneiss dome, Arabian–Nubian Shield

K. ALI*‖, A. ANDRESEN‡†, W. I. MANTON*, R. J. STERN*, S. A. OMAR§ & A. E. MAURICE¶

*Geosciences Department, University of Texas at Dallas, 800 West Campbell Rd, Richardson, TX 75080 USA
‡Department of Geosciences, P. O. Box 1047, University of Oslo, Blindern, O316 Oslo, Norway
§Nuclear Materials Authority, P. O. Box 530, El Maadi, Kattamyia, Egypt
¶Geology Department, Faculty of Earth Science, Beni Suef University, 62517 Beni Suef, Egypt
‖Department of Mineral Resources and Rocks, Faculty of Earth Sciences, King Abdulaziz University, Jeddah 21589, Saudi Arabia

(*Received* 16 February 2011; *accepted* 7 October 2011; *first published online* 16 December 2011)

Abstract – The calc-alkaline, gneissic El Shalul granite is the westernmost gneiss dome or core complex within the Arabian–Nubian Shield. Previous studies have indicated that it represents either a window into the underlying pre-Neoproterozoic Sahara metacraton or a melt derived from the metacraton. U–Pb LA-ICP-MS dating of magmatic zircons from two samples of the variably foliated El Shalul pluton gives ages of 637 ± 5 Ma and 630 ± 6 Ma, excluding it from representing exhumed cratonic rocks. The ages are, however, indistinguishable from the age of the Um Ba'anib pluton, constituting the core of the Meatiq Gneiss Dome, as well as several other plutons in the Eastern Desert, indicating an important magmatic pulse in the Arabian–Nubian Shield in Late Cryogenian time. Major and trace element data indicate a within-plate setting. Bulk rock Nd-isotope and Hf-isotope data on zircons from the El Shalul pluton indicate derivation of the primary melt from a relatively juvenile source, either the lower crust of a mid-Neoproterozoic volcanic arc or as a result of fractionation of a mantle-derived mafic melt. Sm–Nd bulk rock isotopic data indicate a model age of *c.* 720 Ma for the protolith from which the melt was derived. Time-corrected Hf-isotope data obtained on the magmatic zircons indicate that the bulk of the source rock was extracted from the mantle around 810 Ma.

Keywords: Eastern Desert, gneiss dome, geochronology, geochemistry.

1. Introduction

A fundamental problem in Neoproterozoic crustal evolution is the age and origin of the various terranes involved in the East African Orogen (950–550 Ma). This is particularly true for the Arabian–Nubian Shield (ANS) (Fig. 1), which makes up the northern termination of the orogen, a region where geochemical and robust geochronological data on igneous and volcanic rocks are limited. A longstanding geological controversy regarding the Eastern Desert of Egypt, now constituting the western part of the ANS, has been the origin of the lower and middle crust. Some authors have argued that the island arc volcanic and volcaniclastic sequences, ophiolite fragments and various types of deformed and undeformed granitoids exposed in the Eastern Desert today are underlain by the extended eastern margin of the pre-Neoproterozoic Sahara metacraton of Abdelsalam, Liégeois & Stern (2002). Sheared granitoids, appearing as gneiss domes structurally below the arc and ophiolite sequences, are by some interpreted to represent 'exposures' of this older, pre-Neoproterozoic basement ('pre-Pan-African') (e.g. El-Gaby, El-Nady & Khudeir, 1984; El-Gaby, List & Tehrani 1988, 1990; Khudeir *et al*. 2008). Others argue that Eastern Desert basement rocks are entirely juvenile and that they formed in an intra-oceanic arc setting within the Mozambique Ocean, or along one or more magmatic arcs along the western margin of the Mozambique Ocean prior to the final collision of East and West Gondwana ∼ 630 Ma (El-Ramly *et al*. 1984; Greiling, Kröner & El-Ramly, 1984; Kröner *et al*. 1987; Greiling *et al*. 1988, 1994; Stern, 1994).

Recent geochronological and Sr–Nd isotopic studies of igneous rocks exposed in the Meatiq Gneiss Dome, one of several gneiss domes in the Central Eastern Desert (Fig. 1), did not support the presence of pre-Neoproterozoic basement in the core of this dome (Andresen *et al*. 2009; Liégeois & Stern, 2010). To further investigate the idea that highly sheared granitoids represent exposures of an older basement, we studied the gneissic El Shalul granite, located west of the Meatiq Dome (Fig. 1), also interpreted as a dome involving pre-orogenic basement rocks (Hamimi, El Amawy & Wetait, 1994). This gneissic body lies at the western edge of exposed pre-Cretaceous basement in the Eastern Desert of Egypt, and the eastern edge of the Saharan metacraton might be identified here. We tested this idea with geochemical, isotopic and geochronological analyses and the results are reported below.

†Author for correspondence: arild.andresen@geo.uio.no

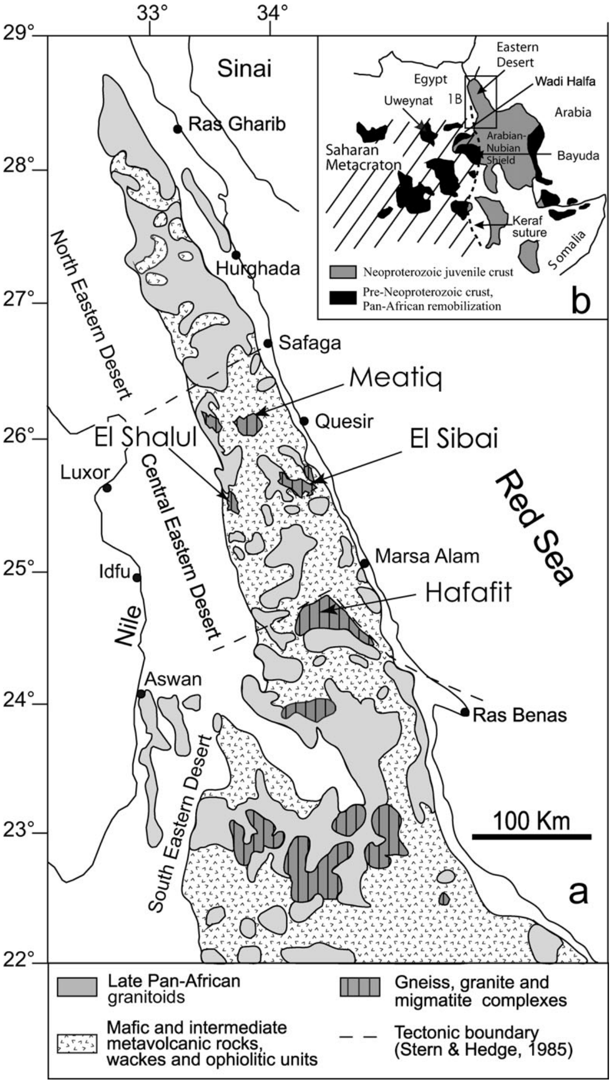

Figure 1. Geological sketch map of the Eastern Desert of Egypt (a) and its position within the Arabian–Nubian Shield (b).

2. Regional geology

The Eastern Desert of Egypt comprises variably deformed and metamorphosed sedimentary, volcanic and plutonic rocks of Precambrian age, unconformably overlain by Cretaceous sediments. The Precambrian basement rocks are particularly well exposed in the Eastern Desert owing to uplift adjacent to the Red Sea (Fig. 1). Similar basement rocks are also exposed along the Saudi Arabian side of the Red Sea, and compose, together with the Egyptian basement rocks, the northern part of the ANS. Deformation and metamorphism of sedimentary, volcanic and plutonic rocks within the ANS are associated with the Neoproterozoic East African orogeny. The transition from juvenile Neoproterozoic rocks exposed on both sides of the Red Sea to older cratonic rocks further west (Sahara metacraton) is poorly constrained (Sultan *et al*. 1994; Abdelsalam, Liégeois & Stern, 2002). However, based on the appearance of several gneiss domes (Meatiq, Sibai, Migif-Hafafit, El Shalul), it has been argued that the Sahara metacraton extends almost as far east as the Red Sea. Mesoproterozoic or older rocks have not been documented in the Eastern Desert of Egypt or the Midyan terrane of northwestern Saudi Arabia, but are present in several terranes in the southern Arabian Shield and Yemen (East Gondwana) (Stacy & Agar, 1985; Whitehouse *et al*. 1998, 2001; Whitehouse, Stoeser & Stacey, 2001; Stoeser & Frost, 2006) (Fig 1).

Despite the lack of robust radiometric ages, most geoscientists accept a three-fold division of the Eastern Desert basement rocks based on their lithology, structural and stratigraphic position, and metamorphic grade. The three tiers or tectonostratigraphic units are from base upwards: (1) high-grade gneisses, (2) the eugeoclinal allochthon (Andresen *et al*. 2010) of arc-type volcanic and volcanosedimentary units, along with variously dismembered ophiolites and (3) the Ediacaran Hammamat and Dokhan supracrustal sequences. A plethora of plutons intrude all three units.

Interbedded with the island arc volcanic and volcanosedimentary rocks of ‘tier 2’ are diamictites, most likely of glacigenic origin, and banded iron-ore formations (BIF) (Stern 1994; Stern *et al*. 2006; Ali *et al*. 2009). The metamorphic grade of the eugeoclinal allochthon does generally not exceed greenschist facies, and this rock assemblage has in previous literature often been referred to as the ‘Pan-African nappes’. The high-strain zone separating the eugeoclinal allochthon from the underlying high-grade metamorphic gneisses is hereafter referred to as the Eastern Desert Shear Zone (EDSZ) (Andresen *et al*. 2010). A protolith age of *c*. 750 Ma is inferred for the volcanic and volcanosedimentary rocks (Ali *et al*. 2009), whereas an age of 736 Ma, interpreted as the age of formation, has been obtained for the Fawakhir ophiolite gabbro (Andresen *et al*. 2009).

Amphibolite grade granitoid gneisses dominate ‘tier 1’ but it also includes mafic and ultramafic rocks. They are locally migmatized. These gneisses, which appear in the core of several gneiss domes (e.g. Meatiq, Hafafit, El Shalul, Fig. 1) throughout the Central Eastern Desert, have been interpreted as representing exposures of the Sahara metacraton (El-Gaby, List & Tehrani, 1990; Khudeir *et al*. 1995, 2008). Recent U–Pb isotope dilution thermal ionization mass spectrometry (ID-TIMS) and Sr–Nd isotopic data from the Meatiq, Sibai and Hafafit areas, however, do not support this interpretation (Bregar *et al*. 2002; Andresen *et al*. 2009; Lundmark *et al*. 2009; Liégeois & Stern, 2010; Augland, Andresen & Boghdady, 2011).

Unconformably on top of the deformed and metamorphosed rocks of the eugeoclinal allochthon are the Hammamat group and Dokhan volcanics of ‘tier 3’. The Hammamat group, composed of sandstone, conglomerate and siltstone, is interpreted to have been deposited in local late-orogenic basins (molasse basins) (Abdeen & Greiling, 2005). The interfingering of volcanic flows/pyroclastic deposits and clastic sediments in the lower part of the Hammamat group has by some been taken in support of a rift-related origin for the molasse basins exposed in the North

https://doi.org/10.1017/S0016756811000975 Published online by Cambridge University Press

Eastern Desert (Stern, Gottfried & Hedge, 1984), and Hammamat sediments were shed south to be deposited in basins in the Central Eastern Desert. U–Pb dating of clastic zircons from the Hammamat group indicates that its depositional age cannot be older than *c*. 600 Ma (Wilde & Youssef, 2002). A similar extrusive age is also obtained on the Dokhan volcanic rocks (Wilde & Youssef, 2000). Breitzkreutz *et al*. (2010) have, however, argued that the two main pulses of Dokhan volcanic activity date to 630–623 Ma and 618–592 Ma. The Hammamat group is in most places folded, indicating a late- rather than post-orogenic setting.

Variably deformed igneous rocks, including undeformed plutonic rocks, occur throughout the Eastern Desert. Their emplacement/crystallization ages are generally poorly constrained. A relative chronology for different plutons has been proposed, based on a combination of degree of deformation (sheared v. non-sheared) and chemical characteristics (e.g. Younger v. Older Granites; Akaad & Noweir, 1980; Greenberg, 1981). Preliminary results from an ongoing dating programme on igneous rocks from the Eastern Desert indicate that this approach should be abandoned (Lundmark *et al*. 2011).

The existing age data on plutonic and meta-plutonic rocks in the Central Eastern Desert range between 710 and 540 Ma (Stern & Hedge, 1985; Kröner, Krüger & Rashwan, 1994; Andresen *et al*. 2009; Lundmark *et al*. 2009, 2011; Augland, Andresen & Boghdady, 2011). The oldest reliable ages (710–680 Ma) are linked to the structurally deepest part of some gneiss domes in the Hafafit-Megif area; this overlaps with the 685–665 Ma episode identified by Stern & Hedge (1985). However, a similar age, on undeformed intrusive rocks (Sukkari pluton, Dabur intrusive complex), is also present in the eugeoclinal allochthon (Lundmark *et al*. 2009, 2011; Pease *et al*. 2010). Two other magmatic pulses also affected the Central Eastern Desert: one around 635–630 Ma (which overlaps with the 625–610 Ma episode of Stern & Hedge, 1985); the other between 609 and 600 Ma (Andresen *et al*. 2009; Lundmark *et al*. 2009, 2011) (which overlaps with the 600–575 Ma episode of Stern & Hedge, 1985). These magmatic events are contemporaneous with top-to-the-NW shearing along the EDSZ (Andresen *et al*. 2009, 2010). Emplacement of the Um Ba'anib granite in the core of the Meatiq Gneiss Dome belongs to the 635–630 Ma magmatic event. Clearly younger than this magmatic pulse is the emplacement of several leucocratic A-type granites around 595–590 Ma. Emplacement of these leucogranites post-dates folding of the Hammamat group. Still younger (550–540 Ma) are some small circular anorthosite–leucogabbro bodies, interpreted to be clearly post-orogenic with respect to the East African orogeny (Augland, Andresen & Boghdady, 2011). As only a limited number of robust absolute age dates exist from the Eastern Desert it is a bit premature to speculate on the plate tectonic significance of the magmatic pulses mentioned above.

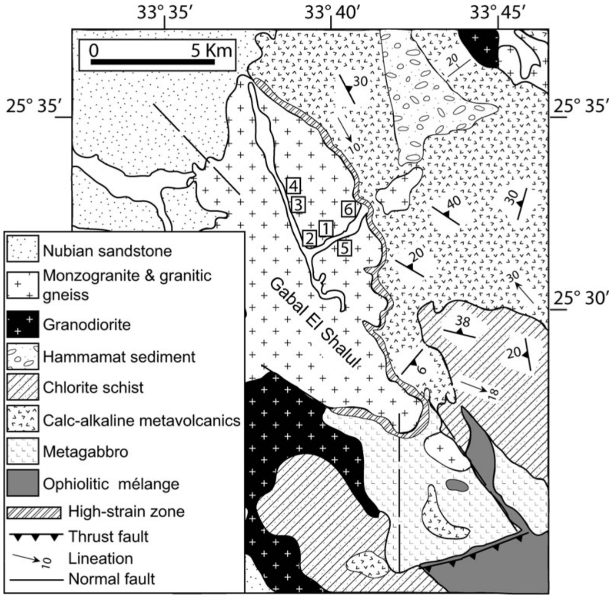

Figure 2. Simplified geological map of the Gabel El Shalul area showing the approximate location of the collected and analysed samples.

3. Geology of the El Shalul area

Gabal El Shalul represents one of the westernmost deformed plutons (El Shalul granitoid) in the Central Eastern Desert forming a NW–SE-trending antiform (Figs 1, 2). The core of the variably deformed granitoid is dominated by monzogranite, whereas granitic gneisses are more common structurally upwards and away from the core. Enclaves of monzogranite in the deformed granites show the granite to be the younger of the two (Hamimi, El Amawy & Wetait, 1994). The dominant structural feature within the gneiss dome is a NW–SE-trending mineral lineation. Isoclinal folds with hinge-lines trending NW–SE are also observed. A high-strain zone separates the El Shalul granitoid from the structurally overlying ophiolitic melange, composed of tectonic blocks of meta-ultramafite, pyroxenite and metagabbro. A detailed petrographic description of the various tectonic blocks in the ophiolitic melange can be found in Z. Hamimi (unpub. Ph.D. thesis, Cairo Univ., 1992), Hamimi, El Amawy & Wetait (1994) and Osman (1996). The melange is overlain tectonostratigraphically by basic to intermediate volcanic rocks, including pillowed basalts and andesites. The ophiolitic melange and volcanic rocks are succeeded by volcanigenic metasediments, including deformed flat pebble conglomerates interbedded with grey phyllite, mudstone and graded greywackes. The above units have all undergone greenschist grade metamorphism prior to emplacement of a granodiorite (Ries *et al*. 1983; Osman 1996). Ragab, El Kalioubi & El Alfy (1983) interpreted the volcanic and volcaniclastic rocks to be part of a magmatic arc.

The Hammamat group sediments, exposed a few kilometres northeast of Gabal El Shalul (Fig. 2), are separate from the underlying ophiolitic melange and

https://doi.org/10.1017/S0016756811000975 Published online by Cambridge University Press

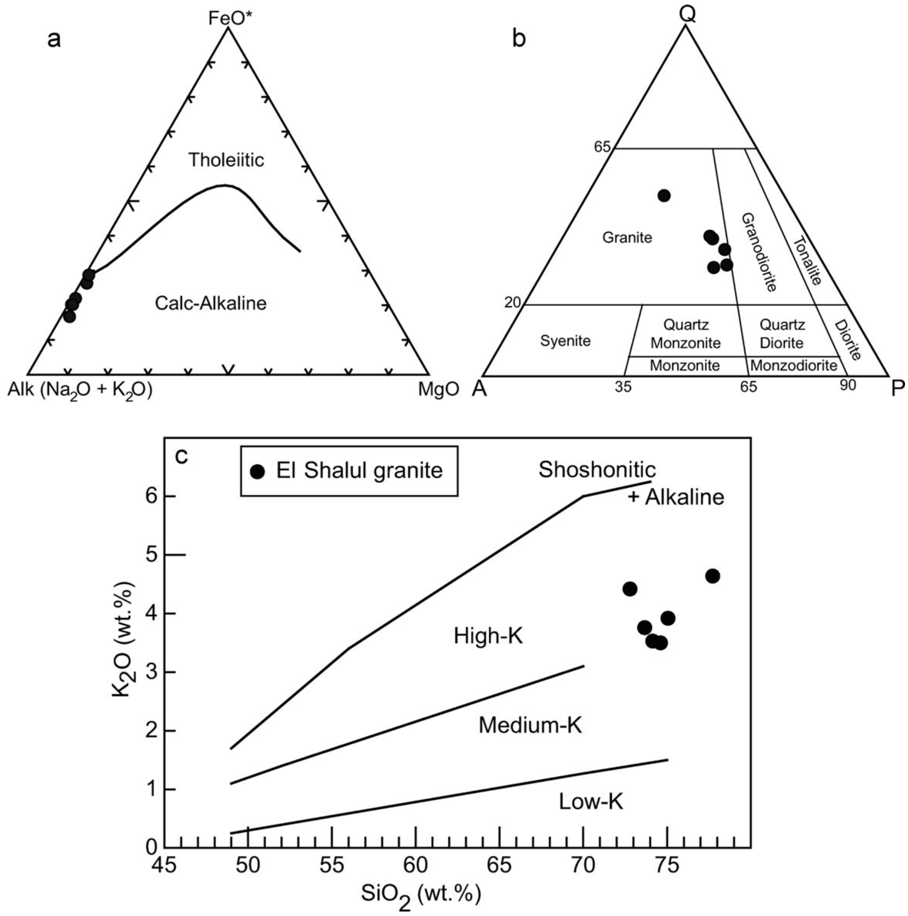

Figure 3. Major and trace element data on samples from the El Shalul granite plotted in some commonly used variation diagrams. (a) (K_2O+Na_2O)–MgO–FeO (AFM) plot (boundary from Irvine & Baragar, 1971). (b) Classification (normative) of the El Shalul pluton based on data given in Table 1. (c) SiO_2 v. K_2O (boundaries from Peccerillo & Taylor, 1976).

volcanic/volcaniclastic rocks by an unconformity. The Hammamat sediments are dominated by poorly sorted conglomerates and sandstone, and the clast petrography (e.g. pebbles derived from the arc terrane and alkali feldspar granite clasts) suggests that the sediments were sourced from the nearby substratum (Osman, 1996). Younger than the Hammamat weakly deformed sediments are undeformed granodiorites and granites, not shown on the simplified geological map (Fig. 2).

Hamimi, El Amawy & Wetait (1994) interpreted the high-strain zone (El Shalul shear zone) separating the eugeoclinal rocks (=ophiolite melange + island arc sequence) from the underlying orthogneisses to have developed during NW to WNW thrusting of the former. The El Shalul shear zone is *c*. 10 m wide and characterized by a mix of foliated metasediments and lenses of mylonitic granite, and it post-dates folding and cleavage development on the structurally overlying eugeoclinal rocks. This shear zone is most likely a westward continuation of the EDSZ described by Andresen *et al*. (2010) from the Meatiq area. However, no carapace of amphibolite grade garnet-bearing metasediments similar to those found below the eugeoclinal allochthon in the Meatiq area has been recognized in the El Shalul area. A second deformational event (D2) folds the dominant foliation in both the El Shalul granite and the eugeoclinal allochthon. Development of NE–SW-trending fold hinges is typical of this event. Post-dating the D2 deformational events is the emplacement of minor volumes of late undeformed gabbros and muscovite granites in the eugeoclinal allochthon (Osman, 1996). It is not known if these late intrusive rocks post-date deposition of the Hammamat sediments, which appear a few kilometres N and NE of the El Shalul granite (Fig. 2). No robust age data exist from the El Shalul granite, but Osman (1996) quotes a Rb–Sr whole-rock age of 670 Ma for the younger pink El Shalul granite.

Osman (1996) describes the ‘post-collisional’ granites of the El Shalul area as composing two large plutons: the El Shalul pluton (Fig. 2) and the El Hassanawia pluton to the north of the area shown in Figure 2. Both are pink and composed of quartz, perthitic K-feldspar, plagioclase and minor biotite. Normative composition of El Shalul granite places it in the monzogranite field (Fig. 3b). The El Hassanawia pluton also contains amphibole. The boundary and age relationship between the two plutons is, however, unclear. Bulk rock geochemical data show the granites to have a calc-alkaline signature and Osman (1996) argues that they formed in a compressional environment.

To test the idea that the El Shalul granite represents a pre-Neoproterozoic basement or was derived by partial melting of a pre-Neoproterozoic basement, we have

https://doi.org/10.1017/S0016756811000975 Published online by Cambridge University Press

carried out Nd- and Sr-isotope studies on bulk rock samples, and U–Pb dating and Lu–Hf isotopic analyses of zircons from the pluton. We also present new major and trace element data for six samples of the El Shalul granitoid.

4. Analytical techniques

Six samples (*c*. 1–2 kg each) of El Shalul granite were collected (Fig. 2). These were analysed for major and trace elements and four were also analysed for Nd and Sr whole-rock isotopic compositions. The following is a brief synopsis of the analytical procedure.

Powders were prepared at University of Texas at Dallas (UTD) and analysed for major elements using fusion inductively coupled plasma whole-rock techniques at ACTLABS, Canada. Trace elements were analysed by inductively coupled plasma mass spectrometry (ICP-MS) using 4-acid digestion (Group 1T-Ms) at ACME Labs, Canada. Table 1 shows the results for major and trace elements from the El Shalul granite.

Whole-rock Nd and Sr isotopic determinations were performed for four granitic samples using the MAT 261 mass spectrometer at UTD. Analytical procedures are described in detail by Hargrove *et al*. (2006). Nd analytical runs consisted of ten blocks of ten scans each for unknowns; four analyses of the La Jolla Nd standard during the time of these analyses yielded a mean $^{143}Nd/^{144}Nd = 0.511857 \pm 0.000014$. Sr analytical runs consisted of 5 blocks of 20 scans each; five analyses of NIST SRM 987 standard yielded mean $^{87}Sr/^{86}Sr = 0.710262 \pm 0.000017$. Calculation of Nd T_{DM} model ages was done following DePaolo (1981, 1983). Analytical results are listed in Table 2.

Zircons for U–Pb dating and Hf-isotope analysis were separated from two rock samples, one strongly foliated (granitic gneiss) the other being a weakly deformed monzogranite, by standard methods including crushing, milling, heavy liquid and Franz magnetic separation at UTD. Hand-picked zircons were mounted in epoxy and a small window exposed by polishing in order to maximize ablation times. Before analysis, all grains were imaged by cathodoluminescence using the scanning electron microscope (SEM-CL) at the Department of Geosciences, University of Oslo.

U–Pb and Lu–Hf-isotope compositions were analysed by laser ablation inductively coupled plasma source mass spectrometry (LA-ICP-MS) using a NU Plasma HR mass spectrometer and a New Wave LUV213 laser microprobe at the Department of Geosciences, University of Oslo. The analytical protocols described in detail by Rosa *et al*. (2009) and Andersen *et al*. (2009) were used for U–Pb geochronology of zircon, and those of Heinonen, Andersen & Rëmö (2010) for Lu–Hf. One to three calibration standards were run in duplicate at the beginning and end of each analytical session, and at regular intervals during sessions. Raw data from the mass spectrometer were corrected for background, laser-induced elemental fractionation, mass discrimination and drift in ion counter gains, and reduced to U and ^{206}Pb concentrations and U–Pb isotopic calibrations to reference zircons of known age.

Table 1. Major and trace element data for El Shalul granite, Egypt

Sample	SH-1	SH-2	SH-3	SH-4	SH-5	SH-6
SiO_2	74.15	74.61	75.06	73.67	72.79	77.73
TiO_2	0.285	0.194	0.238	0.278	0.224	0.221
Al_2O_3	12.65	12.16	12.44	13.41	13.24	11.92
Fe_2O_3	3.46	2.51	2.23	3.37	2.52	1.51
MnO	0.071	0.045	0.007	0.07	0.011	0.013
MgO	0.19	0.10	0.05	0.06	0.09	0.17
CaO	0.71	0.48	0.46	0.29	0.48	0.36
Na_2O	5.09	4.41	3.87	3.79	4.39	1.92
K_2O	3.52	3.50	3.92	3.76	4.42	4.64
P_2O_5	0.04	0.03	0.03	0.04	0.03	0.03
LOI	0.43	0.23	0.41	0.52	0.43	1.31
Total	100.6	98.28	98.73	99.26	98.62	99.84
Mo	2.14	2.05	1.68	5.06	4.45	13.93
Cu	22.27	13.26	16.26	8.44	7.53	7.49
Pb	10.06	11.38	10.09	19.84	6.03	22.09
Zn	173	131.8	75.4	119.7	101.5	46.7
Ag*	46	27	77	81	30	374
Ni	25.5	13.5	12.5	6.2	7.2	2.8
Co	2.0	1.0	1.3	1.3	1.0	0.6
U	1.6	1.5	2.1	1.6	2.7	4.2
Th	5.9	5.4	6.7	5.1	10.1	7.5
Au	< 0.1	< 0.1	< 0.1	< 0.1	< 0.1	< 0.1
Rb	59.7	59.3	68.5	72.4	91.3	95.0
Sr	23	16	19	34	22	23
Cd	0.31	0.41	0.11	0.16	0.22	0.17
Sb	0.40	0.31	0.23	0.50	0.21	0.18
Bi	0.12	0.09	0.12	0.16	0.12	2.24
V	2.00	2.00	2.00	3.00	2.00	6.00
La	78.2	61.6	79.1	67.6	82.2	61.7
Cr	61	32	31	18	12	11
Ba	450	541	486	679	462	396
W	1.2	1.3	0.7	2.1	2.3	2.1
Zr	123	163	214	138	249	340
Sn	5.5	6.7	6.1	10.3	3.4	9.3
Be	5.00	5.00	9.00	3.00	8.00	3.00
Sc	1.40	1.10	1.00	1.50	0.80	1.20
Y	66.2	66.8	48.9	49.3	56.4	38.8
Ce	167.1	137.1	155.0	156.4	186.6	130.0
Pr	22.5	17.5	22.6	19.6	24.3	18.3
Nd	93.0	71.1	92.5	80.9	98.6	73.9
Sm	16.5	13.5	17.9	14.5	17.1	15.2
Eu	2.6	2.2	2.5	2.3	1.9	1.8
Gd	14.0	13.7	14.7	12.2	12.7	12.7
Tb	2.5	2.1	2.1	1.8	2.1	1.8
Dy	14.6	13.6	11.8	10.7	11.8	9.6
Ho	3.0	2.9	2.3	2.2	2.4	1.8
Er	8.2	7.8	6.4	6.3	6.9	5.5
Tm	1.1	0.9	0.8	0.9	0.9	0.8
Yb	7.4	6.7	6.5	6.9	6.6	5.9
Lu	1.1	1.1	0.9	1.0	0.9	0.9
Hf	3.92	5.16	6.07	4.27	8.35	11.45
Li	40.4	20.4	1.00	5.3	1.9	9.8
Ta	2.1	2.2	3.3	2.1	4.4	3.5
Nb	43.6	45.7	66.4	44.2	89.9	84.9
Cs	0.8	0.7	0.7	0.5	0.4	0.8
Ga	24.4	24.4	25.2	25.3	28.5	28.9

Major elements in wt %; trace elements in ppm and *ppb

5. Results

5.a. Major and trace element geochemistry

Major and trace element data obtained on the six samples is presented in Table 1. The geochemical data show limited compositional variation, with the

https://doi.org/10.1017/S0016756811000975 Published online by Cambridge University Press

Table 2. Sm/Nd and Rb/Sr and isotopic data for El Shalul granite, Egypt

Sample	Rb (ppm)	Sr (ppm)	$^{87}Rb/^{86}Sr$	$^{87}Sr/^{86}Sr \pm 2\sigma$	$^{87}Sr/^{86}Sr$ (initial)	Sm (ppm)	Nd (ppm)	$^{147}Sm/^{144}Nd$	$^{143}Nd/^{144}Nd \pm 2\sigma$	$\varepsilon_{Nd}(t)$	T_{DM} (Ma) (Goldstein *et al.* 1984)	T_{DM} (Ma) (DePaolo, 1981)
SH-1	59.7	22	7.85	0.773494 ± 57	0.702483	16.50	93.00	0.1072	0.512605 ± 10	6.62	782	641
SH-2	59.3	16	10.72	0.811870 ± 75	0.714885	13.50	71.10	0.1147	0.512645 ± 31	6.79	780	628
SH-5	91.3	22	12.01	0.819646 ± 12	0.711049	17.10	98.60	0.1048	0.512635 ± 11	7.40	723	586
SH-6	95.0	23	11.95	0.813455 ± 66	0.705370	15.20	73.20	0.1243	0.512722 ± 12	7.52	732	567

All isotopic analyses conducted at YT Dallas on a Finnigan Mat 261 solid source instrument. Trace element concentrations determined at AcmeLabs, Canada.
Model ages based on DePaolo (1981) and Goldstein *et al.* (1984). Errors reported for isotopic ratios are 2σ. $\varepsilon_{Nd}(t)$ and Sr(i) were calculated for an age of 634 Ma.
Mean value of La Jolla standards is $^{143}Nd/^{144}Nd = 0.512857 \pm 0.000014$ and NIST SRM 987 standards is $^{87}Sr/^{86}Sr = 0.710262 \pm 0.000017$.

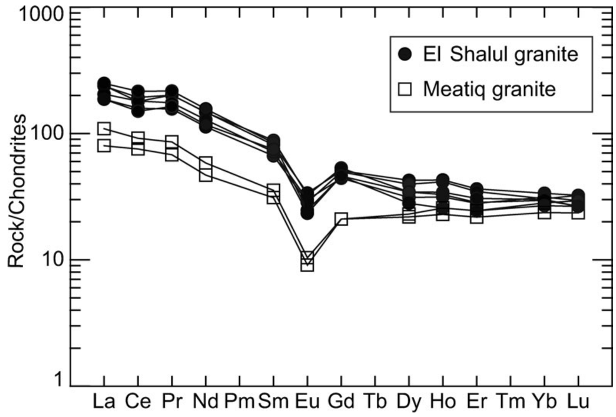

Figure 4. REE diagrams of bulk rock samples from the El Shalul granite. Relevant data from the Meatiq Gneiss Dome are also plotted for comparison. All elements are normalized to the values of chondrites reported by Nakamura (1974).

exception of sample SH-6. Chemical variation diagrams (Fig. 3a, c) show the El Shalul granites to be rich in alkalis, belonging to the high-K calc-alkaline or alkaline suites (Le Maitre *et al.* 1989). The studied rocks show that the El Shalul granite is enriched in rare earth elements (REEs) relative to chondrites, especially light rare earth elements (LREEs) (Fig. 4), and displays a typical high-K calc-alkaline granite pattern. When the data are plotted in commonly used discrimination diagrams, the El Shalul granite shows the characteristics of an A-type (Whalen, Currie & Chapell, 1987; Fig. 5a) or within-plate granite (Pearce, Harris & Tindle, 1984; Fig. 5b). A-type granites contain low Al_2O_3, MgO, CaO, TiO_2, Sr and Ba and high Rb, Nb and Y (Moghazi, 2002). They are commonly thought to be late- to post-tectonic.

5.b. U–Pb zircon geochronology

From a large population of extracted zircons, 50 grains from sample SH-1 and 35 grains from sample SH-6 were hand-picked for SEM-CL imaging. Of these, 20 SH-1 grains and 22 SH-6 grains were chosen for LA-ICP-MS analysis to obtain U–Pb ages and $^{176}Hf/^{177}Hf$ ratios on the individual zircons. The obtained U–Pb and $^{176}Hf/^{177}Hf$ data are presented in Tables 3 and 4. Further details on mineral separation and analytical procedures are given in Section 4.

All analysed grains show well-developed oscillatory zoning in SEM-CL images (Fig. 6), typical for zircons crystallizing out of a melt (Corfu *et al.* 2003). None of the studied grains showed overgrowths on an older rounded, inherited core. Zircons from both samples were low in uranium and ^{206}Pb (∼ 50 ppm and ∼ 5 ppm, respectively). Most analysed grains are concordant (< 10 % of central concordance) when plotted on a concordia diagram (Fig. 7). SH-1 has a concordia age of 637 ± 5 Ma and SH-6 has an age of 631 ± 6 Ma based on calculation procedures proposed by Ludwig (1998, 2003). These are interpreted as magmatic crystallization ages for the El Shalul granite. The two obtained ages overlap within error and the

https://doi.org/10.1017/S0016756811000975 Published online by Cambridge University Press

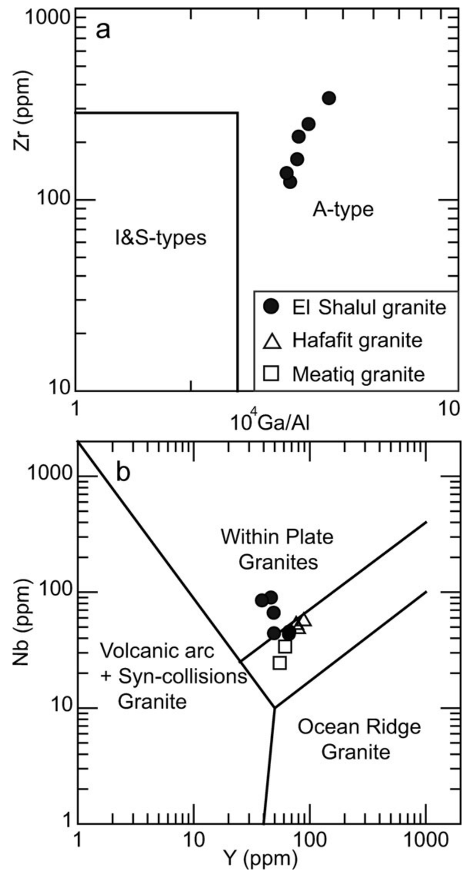

Figure 5. Trace element data from the El Shalul granite samples plotted in tectonic discrimination diagrams (boundaries from (a) Whalen *et al.* 1987 and (b) Pearce *et al.* 1984). Data from the Meatiq and Hafafit gneiss domes are from Liégeois & Stern (2010).

El Shalul granite age is hereafter given as 634 Ma. One cannot, however, exclude the possibility that the age difference is real and results from two pulses of zircon crystallization/magma emplacement within the El Shalul granite. The latter interpretation is supported by the compositional difference between SH-6 and the other five samples.

5.c. Sr-, Nd- and Hf-isotope geochemistry

To evaluate the crustal residence time and chemical characteristics of the El Shalul granite source rock we have obtained $^{143}Nd/^{144}Nd$ and $^{87}Sr/^{86}Sr$ ratios on four bulk rock samples, and $^{176}Hf/^{177}Hf$ on 42 zircon grains, 20 from SH-1 and 22 from SH-6, most of which had already been dated. The data are presented in Tables 2 and 4.

All the $^{147}Sm/^{144}Nd$ ratios are < 0.14, so the Nd T_{DM} are considered meaningful (Küster *et al.* 2008). The ε_{Nd} values for the four samples (SH-1, SH-2, SH-5 and SH-6, each calculated using a crystallization age of 634 Ma) vary between +7.5 and +6.6 with a mean of +7.1 indicating derivation of the El Shalul granite from a source with a time-integrated depletion in LREEs, as monitored by Sm/Nd. This is consistent with the interpretation that Nd evolved in a strongly depleted, upper mantle-like chemical reservoir prior to the Neoproterozoic. The mean ε_{Nd} plots very close to the depleted mantle evolution curve of Nelson & DePaolo (1985) at 634 Ma (Fig. 8). This indicates that the source rock for the El Shalul magma had a very short crustal residence time. If the depleted mantle evolution curve of Goldstein *et al.* (1984) is used instead, a slightly longer crustal residence time (and older T_{DM}) is allowed. But the difference is less than 200 Ma ($T_{DM} < 800$ Ma). If pre-Neoproterozoic crustal rocks had been the source for the El Shalul magma a negative ε_{Nd} value would be expected, which is not found. The Nd model ages for the four granitic samples yield T_{DM} ages from 567 to 641 Ma (model of DePaolo, 1981) and from 723 to 782 Ma (model of Goldstein *et al.* 1984; Table 2). The Nd model ages (mean = 606 Ma, model of DePaolo, 1981) are about the same as the U–Pb zircon crystallization age (634 Ma). The $^{87}Rb/^{86}Sr$ ratios obtained on the four samples analysed (Table 2) are very high (7.8 up to 12), most likely due to alteration, which prevents a precise calculation of Sr initial ratios.

The use of Lu–Hf radiogenic isotope system gives information that in many respects duplicates that provided by the Sm–Nd system (Dickin, 2005). As a tracer of petrogenetic processes, however, Lu–Hf has one important advantage over Sm–Nd: zircons retain a robust memory of their initial Hf isotopic compositions owing to their high Hf concentrations, low Lu/Hf ratios and general ability to survive metamorphic processes. Zircons also have the advantage of being datable by the U–Pb techniques.

Zircon Hf isotopic compositions are presented in Table 4. The measured $^{176}Lu/^{177}Hf$ ratios are used to calculate initial $^{176}Hf/^{177}Hf$. For the calculation of ε_{Hf} we have adopted the chondritic values of Blichert-Toft & Albarède (1997). To calculate model ages based on a depleted mantle source, we have adopted a model with $(^{176}Hf/^{176}Hf)_i = 0.279718$ and $^{176}Lu/^{177}Hf = 0.0384$ (Griffin *et al.* 2000, 2002; Andersen, Griffin & Person, 2002). This produces over 4.56 Ga a value of $^{176}Hf/^{177}Hf$ (0.28325) similar to that of average present-day mid-ocean ridge basalt (MORB). This mantle evolution curve is indistinguishable from the evolution curve of Vervoort & Blichert-Toft (1999).

The time-corrected epsilon values ($\varepsilon_{Hf}(t)$) for the 42 analysed grains vary between +12.0 and +6.1, with an average of 9.3 for SH-1 and 9.2 for SH-6. The depleted mantle model age obtained using a crystallization age of 634 Ma for the zircons, an $\varepsilon_{Hf}(t) = 9.25$ and the mean of measured $^{176}Hf/^{177}Hf$ values gives an age of *c.* 810 Ma. The obtained Hf-isotope data thus indicate that the source for the El Shalul magma cannot have been extracted from the mantle in pre-Neoproterozoic time. This model age suggests that the 634 Ma El Shalul granite was derived from remnants of slightly older juvenile crust. If a fractionated mantle-derived basaltic melt is invoked, incorporation of Mesoproterozoic or older crustal material is very limited.

https://doi.org/10.1017/S0016756811000975 Published online by Cambridge University Press

https://doi.org/10.1017/S0016756811000975 Published online by Cambridge University Press

Table 3. U–Pb data on samples

				Ratios										Ages					
Sample	Grain	U (ppm)	^{206}Pb (ppm)	^{206}Pb/^{204}Pb	^{207}Pb/^{206}Pb	1SE	^{207}Pb/^{235}U	1SE	^{206}Pb/^{238}U	1SE	Rho	Disc. (%)*	Min. rim (%)**	^{207}Pb/^{206}Pb	1σ	^{207}Pb/^{235}U	1σ	^{206}Pb/^{238}U	1σ
UMSH1	7	53	4.2	1113	0.0651	0.0004	0.8539	0.0162	0.0952	0.00170	0.94	−25.7	−22.2	777	13	627	9	586	10
UMSH1	11	34	2.5	499	0.0609	0.0006	0.8147	0.0221	0.0970	0.00246	0.94	−6.7	0	637	20	605	12	597	14
UMSH1	15	61	5.1	662	0.0798	0.0006	1.0757	0.0259	0.0977	0.00224	0.95	−51.9	−50.0	1193	14	742	13	601	13
UMSH1	16	72	6.0	1056	0.0693	0.0005	0.9574	0.0203	0.1002	0.00200	0.94	−33.8	−30.7	908	15	682	11	615	12
UMSH1	5	61	5.4	949	0.0608	0.0004	0.8644	0.0164	0.1031	0.00184	0.94	−0.1	0	633	13	633	9	632	11
UMSH1	2	37	3.9	1379	0.0607	0.0018	0.8635	0.0309	0.1032	0.00198	0.54	0.8	0	628	63	632	17	633	12
UMSH1	9	42	3.7	926	0.0612	0.0005	0.8703	0.0172	0.1031	0.00188	0.93	−2.3	0	647	16	636	9	633	11
UMSH1	8	58	5.0	2800	0.0609	0.0004	0.8676	0.0163	0.1033	0.00181	0.94	−0.6	0	637	14	634	9	634	11
UMSH1	4	55	4.8	1823	0.0606	0.0004	0.8646	0.0166	0.1035	0.00184	0.93	1.7	0	625	15	633	9	635	11
UMSH1	1	37	3.8	831	0.0609	0.0020	0.8692	0.0332	0.1036	0.00201	0.51	0.2	0	634	70	635	18	635	12
UMSH1	20	46	4.1	1309	0.0606	0.0004	0.8673	0.0181	0.1038	0.00204	0.94	1.7	0	626	15	634	10	636	12
UMSH1	12	39	3.4	867	0.0607	0.0004	0.8685	0.0169	0.1038	0.00188	0.93	1.3	0	629	14	635	9	636	11
UMSH1	6	45	4.0	1341	0.0612	0.0005	0.8751	0.0170	0.1037	0.00186	0.92	−1.5	0	646	16	638	9	636	11
UMSH1	18	64	5.6	1532	0.0624	0.0004	0.8928	0.0181	0.1038	0.00198	0.94	−7.9	−2.8	688	14	648	10	636	12
UMSH1	13	45	3.9	1576	0.0607	0.0004	0.8711	0.0170	0.1041	0.00190	0.94	1.6	0	629	14	636	9	638	11
UMSH1	10	39	3.4	2039	0.0609	0.0004	0.8761	0.0173	0.1044	0.00192	0.93	0.9	0	635	15	639	9	640	11
UMSH1	3	37	4.0	1092	0.0603	0.0018	0.8695	0.0321	0.1046	0.00218	0.56	4.7	0	614	62	635	17	641	13
UMSH1	17	40	3.8	1179	0.0608	0.0005	0.8762	0.0184	0.1045	0.00201	0.92	1.2	0	633	18	639	10	641	12
UMSH1	14	39	3.4	1951	0.0620	0.0004	0.8931	0.0185	0.1045	0.00204	0.94	−5.2	0	674	15	648	10	641	12
UMSH1	19	65	6.0	1410	0.0611	0.0005	0.8820	0.0174	0.1048	0.00191	0.92	0.2	0	641	15	642	9	642	11
UMSH6	10	42	3.7	345	0.0737	0.00253	0.8879	0.0346	0.0874	0.00162	0.48	−49.8	−39.7	1034	67	645	19	540	10
UMSH6	11	27	2.1	292	0.0695	0.00078	0.9130	0.0197	0.0952	0.00176	0.85	−37.5	−33.3	914	22	659	10	586	10
UMSH6	2	42	4.3	426	0.0603	0.00164	0.8424	0.0270	0.1013	0.00172	0.53	1.0	0	616	58	620	15	622	10
UMSH6	1	55	5.7	1072	0.0615	0.00219	0.8613	0.0348	0.1016	0.00195	0.47	−5.1	0	656	72	631	19	624	11
UMSH6	5	47	4.9	653	0.0604	0.00185	0.8510	0.0305	0.1022	0.00191	0.52	1.6	0	618	64	625	17	627	11
UMSH6	7	82	8.5	1959	0.0607	0.00183	0.8551	0.0315	0.1022	0.00215	0.57	−0.1	0	628	66	627	17	627	13
UMSH6	13	51	4.4	756	0.0604	0.00044	0.8573	0.0172	0.1029	0.00192	0.93	2.0	0	619	15	629	9	631	11
UMSH6	14	44	3.7	560	0.0605	0.00046	0.8614	0.0179	0.1033	0.00200	0.93	2.0	0	622	15	631	10	633	12
UMSH6	12	46	4.0	1223	0.0606	0.00044	0.8619	0.0179	0.1032	0.00201	0.94	1.6	0	624	15	631	10	633	12
UMSH6	4	43	4.4	368	0.0604	0.00188	0.8615	0.0321	0.1035	0.00213	0.55	2.9	0	618	64	631	18	635	12
UMSH6	15	38	3.4	826	0.0605	0.00048	0.8638	0.0181	0.1035	0.00201	0.93	2.0	0	623	16	632	10	635	12
UMSH6	9	50	5.2	656	0.0602	0.00162	0.8601	0.0277	0.1036	0.00182	0.55	4.3	0	611	55	630	15	636	11
UMSH6	6	43	4.5	712	0.0604	0.00192	0.8637	0.0315	0.1037	0.00184	0.49	3.2	0	617	64	632	17	636	11
UMSH6	3	140	14.7	2303	0.0608	0.00183	0.8690	0.0307	0.1038	0.00191	0.52	1.0	0	630	65	635	17	636	11
UMSH6	8	43	4.5	488	0.0621	0.00176	0.8942	0.0299	0.1044	0.00185	0.53	−5.7	0	677	59	649	16	640	11

* Discordance from the centre of an error ellipse.
** Minimum discordance from the rim of an error ellipse.

https://doi.org/10.1017/S0016756811000975 Published online by Cambridge University Press

Table 4. Lu–Hf data on samples

Sample	Grain	$^{176}Hf/^{177}Hf$	1σ	$^{178}Hf/^{177}Hf$	1σ	$^{176}Yb/^{177}Hf$	1σ	$^{176}Lu/^{177}Hf$	1σ	$\varepsilon_{Hf}(t)$*	2σ	tDM$_z$ (Ga)**	2σ	tDM$_w$ (Ga)***
UMSH1	1	0.282646	0.000012	1.467240	0.000027	0.068232	0.000690	0.001120	0.000054	8.28	0.80	0.86	0.02	1.00
UMSH1	2	0.282716	0.000010	1.467240	0.000037	0.080058	0.000560	0.001285	0.000002	10.69	0.69	0.77	0.01	0.84
UMSH1	3	0.282722	0.000016	1.467180	0.000041	0.104781	0.003100	0.001638	0.000049	10.75	1.09	0.77	0.02	0.84
UMSH1	4	0.282677	0.000012	1.467220	0.000030	0.095730	0.004800	0.001455	0.000067	9.23	0.79	0.83	0.02	0.93
UMSH1	5	0.282714	0.000016	1.467370	0.000043	0.095283	0.002500	0.001481	0.000021	10.53	1.12	0.77	0.02	0.85
UMSH1	6	0.282697	0.000015	1.467230	0.000040	0.125983	0.000580	0.001923	0.000010	9.74	1.05	0.81	0.02	0.90
UMSH1	7	0.282609	0.000008	1.467260	0.000033	0.093168	0.000770	0.001513	0.000001	6.80	0.59	0.92	0.01	1.09
UMSH1	8	0.282702	0.000010	1.467270	0.000035	0.138932	0.001500	0.002159	0.000015	9.82	0.70	0.81	0.01	0.90
UMSH1	9	0.282614	0.000012	1.467280	0.000022	0.064827	0.000450	0.000996	0.000005	7.20	0.85	0.90	0.02	1.06
UMSH1	10	0.282689	0.000016	1.467290	0.000029	0.066458	0.000200	0.000993	0.000006	9.85	1.13	0.80	0.02	0.90
UMSH1	11	0.282642	0.000017	1.467240	0.000032	0.085850	0.002000	0.001322	0.000019	8.05	1.19	0.87	0.02	1.01
UMSH1	12	0.282706	0.000012	1.467300	0.000040	0.093918	0.000840	0.001365	0.000007	10.30	0.84	0.78	0.02	0.87
UMSH1	13	0.282685	0.000008	1.467210	0.000023	0.107725	0.001700	0.001627	0.000006	9.44	0.58	0.82	0.01	0.92
UMSH1	14	0.282705	0.000013	1.467200	0.000035	0.139306	0.001000	0.002061	0.000011	9.97	0.91	0.80	0.02	0.89
UMSH1	15	0.282685	0.000015	1.467270	0.000037	0.117003	0.000760	0.001810	0.000007	9.37	1.06	0.82	0.02	0.93
UMSH1	16	0.282625	0.000014	1.467320	0.000051	0.090634	0.000660	0.001342	0.000035	7.44	0.96	0.90	0.02	1.05
UMSH1	17	0.282660	0.000018	1.467240	0.000046	0.086580	0.000470	0.001310	0.000003	8.69	1.27	0.85	0.03	0.97
UMSH1	18	0.282708	0.000016	1.467250	0.000031	0.102759	0.000990	0.001551	0.000011	10.29	1.12	0.78	0.02	0.87
UMSH1	19	0.282763	0.000019	1.467260	0.000038	0.135175	0.004000	0.002124	0.000056	12.00	1.30	0.72	0.03	0.76
UMSH1	20	0.282644	0.000013	1.467270	0.000033	0.087196	0.000540	0.001291	0.000008	8.14	0.91	0.87	0.02	1.00
UMSH6	1	0.282705	0.000014	1.467260	0.000041	0.086215	0.000560	0.001437	0.000010	10.10	0.98	0.79	0.02	0.87
UMSH6	2	0.282679	0.000012	1.467250	0.000026	0.109141	0.002900	0.001887	0.000048	8.99	0.81	0.83	0.02	0.95
UMSH6	3	0.282680	0.000017	1.467210	0.000029	0.186326	0.000610	0.002955	0.000068	8.58	1.15	0.86	0.02	0.97
UMSH6	4	0.282677	0.000014	1.467240	0.000028	0.106476	0.001400	0.001801	0.000018	8.96	0.98	0.83	0.02	0.95
UMSH6	5	0.282602	0.000012	1.467230	0.000036	0.076811	0.001900	0.001306	0.000027	6.51	0.83	0.93	0.02	1.10
UMSH6	6	0.282660	0.000013	1.467220	0.000030	0.129677	0.004100	0.002192	0.000067	8.19	0.86	0.87	0.02	1.00
UMSH6	7	0.282692	0.000014	1.467230	0.000033	0.178866	0.001400	0.002845	0.000032	9.05	0.96	0.84	0.02	0.94
UMSH6	8	0.282681	0.000012	1.467210	0.000036	0.163127	0.002100	0.002664	0.000061	8.74	0.80	0.85	0.02	0.96
UMSH6	9	0.282704	0.000017	1.467190	0.000028	0.092107	0.000580	0.001514	0.000012	10.04	1.19	0.79	0.02	0.88
UMSH6	10	0.282713	0.000013	1.467240	0.000034	0.172613	0.012000	0.002401	0.000120	9.98	0.82	0.79	0.02	0.88
UMSH6	11	0.282659	0.000013	1.467330	0.000034	0.076344	0.001100	0.001358	0.000032	8.51	0.89	0.85	0.02	0.98
UMSH6	12	0.282701	0.000015	1.467320	0.000036	0.129603	0.005700	0.002055	0.000084	9.70	0.99	0.80	0.02	0.90
UMSH6	13	0.282717	0.000012	1.467200	0.000030	0.112005	0.000770	0.001813	0.000014	10.37	0.84	0.78	0.02	0.86
UMSH6	14	0.282662	0.000010	1.467320	0.000031	0.083913	0.001600	0.001351	0.000016	8.62	0.69	0.84	0.01	0.97
UMSH6	15	0.282676	0.000017	1.467260	0.000038	0.124195	0.001900	0.002150	0.000041	8.78	1.17	0.84	0.02	0.96
UMSH6	16	0.282712	0.000017	1.467320	0.000043	0.235443	0.003500	0.003429	0.000058	9.52	1.16	0.82	0.02	0.91
UMSH6	17	0.282690	0.000013	1.467350	0.000029	0.123565	0.002800	0.001949	0.000051	9.36	0.88	0.82	0.02	0.92
UMSH6	18	0.282842	0.000031	1.467300	0.000058	0.255605	0.006400	0.004183	0.000220	13.80	2.01	0.64	0.04	0.64
UMSH6	19	0.282687	0.000013	1.467210	0.000024	0.105621	0.002000	0.001654	0.000036	9.38	0.89	0.82	0.02	0.92
UMSH6	20	0.282625	0.000015	1.467300	0.000031	0.074023	0.001600	0.001162	0.000019	7.39	1.05	0.89	0.02	1.05
UMSH6	21	0.282663	0.000014	1.467320	0.000044	0.078584	0.000200	0.001254	0.000005	8.69	0.99	0.84	0.02	0.96
UMSH6	22	0.282660	0.000019	1.467420	0.000053	0.109282	0.002700	0.001671	0.000039	8.41	1.31	0.86	0.03	0.98

* $\varepsilon_{Hf}(t)$ calculated using same U–Pb age for all grains within the sample and decay constant 1.867×10^{-11} (Søderlund *et al*. 2004).
** tDM$_z$ is depleted mantle model age calculated using same U–Pb age for all grains within the sample, $^{176}Lu/^{177}Hf$ measured from zircon and DM model by Griffin *et al*. (2000).
*** tDM$_w$ is depleted mantle model age calculated like tDM$_z$, but assuming whole-rock $^{176}Lu/^{177}Hf = 0.015$.

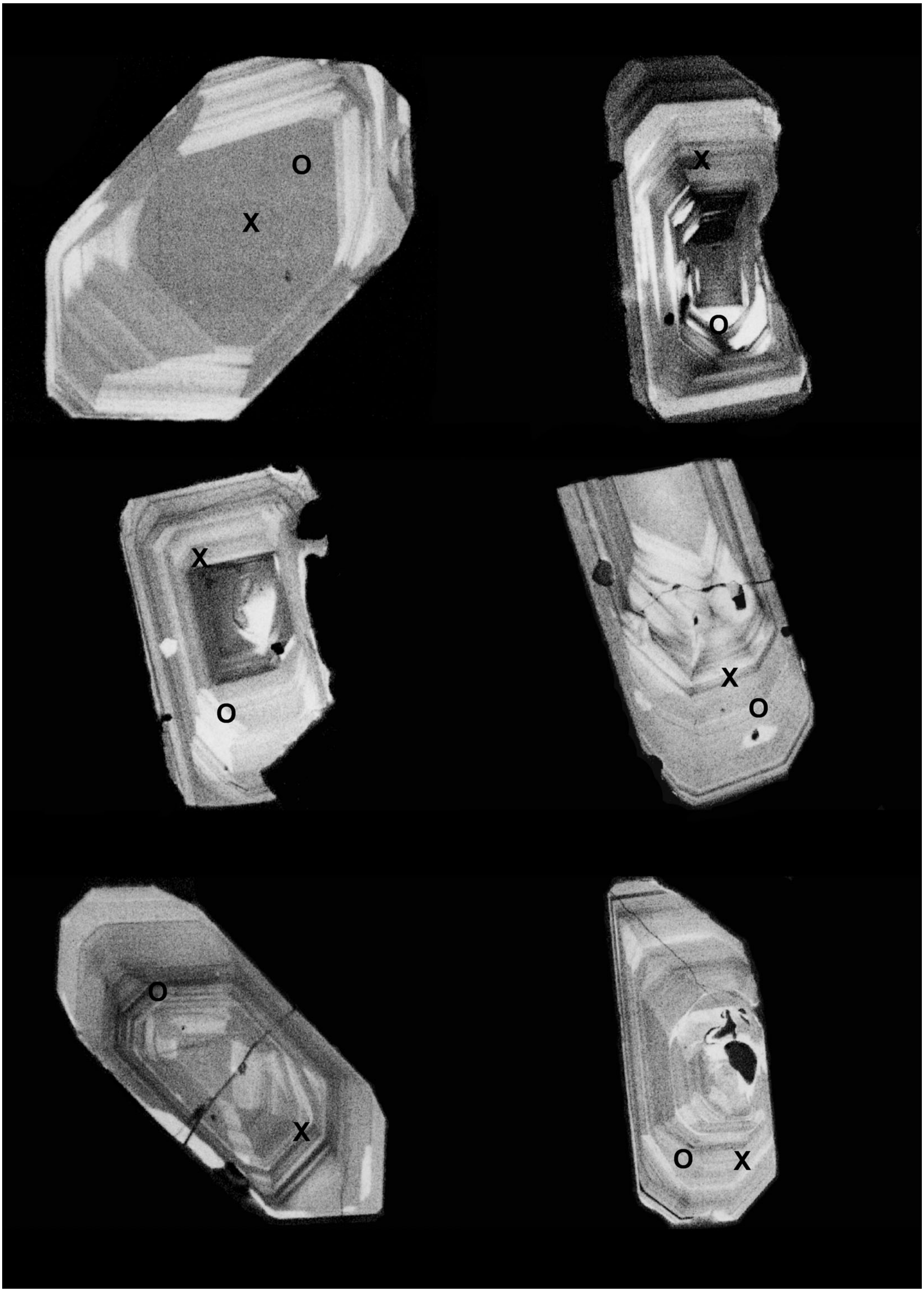

Figure 6. Representative CL images of magmatically zoned zircon crystal from sample SH-6 and SH-6. x and o represent position of the laser for U–Pb and Lu–Hf analyses, respectively.

https://doi.org/10.1017/S0016756811000975 Published online by Cambridge University Press

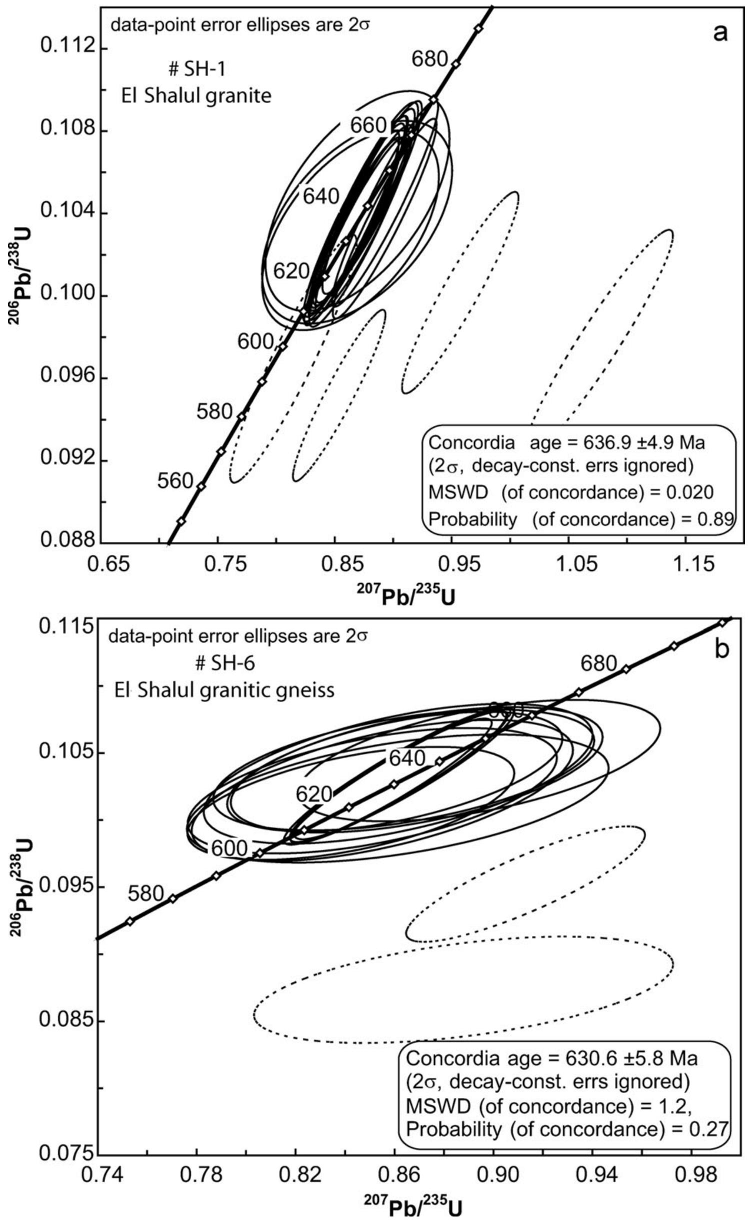

Figure 7. Plot of LA-ICP-MS U–Pb isotope data on zircons from the El Shalul granite samples (SH-1 and SH-6). Dashed ellipses represent discordant analyses that were excluded from age calculations. Analytical data is given in Table 3.

6. Discussion

The geochemical, isotopic and geochronological data presented above show the El Shalul granite to be a high-K-alkaline to calc-alkaline granite with an emplacement age of *c*. 634 Ma. It does not represent a window into the eastern part of the pre-Neoproterozoic Sahara metacraton as argued by Hamimi, El Amawy & Wetait (1994). The obtained age is almost identical to the crystallization age of the gneissic Um Ba'anib granite (631 Ma) making up the core of the Meatiq Gneiss Dome (Andresen *et al*. 2009). Similar ages from the Hafafit and Sibai areas (Lundmark *et al*. 2009, 2011) may indicate that a regionally extensive phase of magma emplacement took place in the Central Eastern Desert of Egypt at *c*. 630–635 Ma.

A controversial issue regarding the evolution of the ANS in Egypt has been the protolith age and composition of the source rocks for the many Neoproterozoic plutons (e.g. Khudeir *et al*. 2008; Liégeois & Stern, 2010). Are the plutons derived from partial melting of pre-Neoproterozoic continental crust or are they juvenile Neoproterozoic crustal additions? The two lines of isotopic evidence presented in the previous Sections demonstrate that the El Shalul granite is derived from a source of Neoproterozoic (1000–542 Ma) age, either by melting of juvenile Neoproterozoic lower crust or fractionation of mantle-derived mafic magmas.

The four time-corrected $\varepsilon_{Nd}(t)$ values obtained in this study are all positive and range between +6.6 and +7.5, (mean = +7.1) indicating derivation from a crustal source that cannot be much older than 700 Ma, if we assume a realistic $^{147}Sm/^{144}Nd$ value (Stern, 2002), the decay constant of ^{147}Sm of 6.54×10^{-12} a^{-1} (Lugmair & Marti, 1978) and the depleted mantle evolution curve

https://doi.org/10.1017/S0016756811000975 Published online by Cambridge University Press

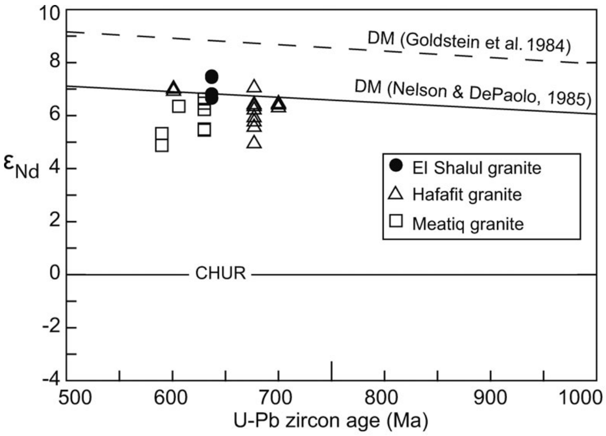

Figure 8. Nd isotopic data on bulk rock samples from the El Shalul granite plotted in a ε_{Nd} v. time (Ma) diagram. The reference lines for chondritic uniform reservoir (CHUR) and the depleted mantle curves (DM) are from Goldstein *et al.* (1984) and Nelson & DePaolo (1985). Nd-isotope data from the Hafafit and Meatiq granites (Hargrove *et al.* 2006; Moussa *et al.* 2008; Liégeois & Stern, 2010) are plotted for comparison.

of Nelson & DePaolo (1985). Significant involvement of pre-Neoproterozoic crust would have resulted in strongly negative ε_{Nd} values, which is not observed. Our $\varepsilon_{Nd}(t)$ data are, however, comparable with recently published $\varepsilon_{Nd}(t)$ (mean = +6.10) on the Um Ba'anib orthogneiss (Liégeois & Stern, 2010), who also argued for a juvenile protolith or parent magma for granitic intrusive rocks in both the Meatiq and Hafafit gneiss domes.

Additional evidences in support of a Neoproterozoic protolith or parent magma age for the El Shalul granite comes from the analysed zircons. If the El Shalul magma was derived from pre-Neoproterozoic continental crust one would expect some inherited zircons to be present, either as cores or as individual, more anhedral grains. Neither has been observed. Derivation of the El Shalul granite from juvenile Neoproterozoic crust or mafic magma is furthermore supported by $\varepsilon_{Hf}(t)$ data from the analysed zircons. There is some spread in the $\varepsilon_{Hf}(t)$ data, but the means (+9.3 and +9.2) for both zircon populations (SH-1 and SH-6) are the same within analytical error. Although there is some disagreement on (i) which depleted mantle curve to use and (ii) which $(^{176}Hf/^{176}Hf)_i$ and $^{176}Lu/^{177}Hf$ ratios to use when calculating model ages (T_{DM}), there is little doubt that the protolith of the El Shalul granite is Neoproterozoic in age. Based on the values used in the calculation, a model age of *c.* 810 Ma is indicated. Keeping in mind the assumption used in the calculations, it is interesting to observe that the Hf model zircon ages are comparable to the Nd model ages recently proposed by Liégeois & Stern (2010), based on bulk rock samples. In their paper they estimated a mean model age of 710 ± 60 Ma (1 sigma) for the protoliths of the Meatiq and Hafafit gneiss domes granitoids. Collectively, we see no evidence for a pre-Neoproterozoic protolith for the El Shalul granite. Continental crustal rocks older than 634 Ma may be involved, but any such component is likely to be early Neoproterozoic in age. In light of the data presented by Liégeois & Stern (2010) and our data it could be *c.* 800 Ma old island arc rocks.

Finally, it should be mentioned that the age of the El Shalul granite (634 Ma) puts an age constraint on top-to-the-NW/NNW displacement of the eugeoclinal allochthon. How much northwestward translation the eugeoclinal allochthon has undergone prior to 634 Ma, and how far it has been displaced remains to be investigated. The precise age of shearing is not known, but must be younger than the emplacement of the El Shalul pluton. How much younger is not clear, as plutons cutting across the mylonitic foliation in the study area have not been dated. However, syn-tectonic plutons in the high-strain zone above the Um Ba'anib orthogneiss some 10 km away have given emplacement ages between 610–604 Ma. Post-tectonic plutons (Um Had, Arieki and Fawakhir granites) in the latter area range between 600 and 590 Ma (Andresen *et al.* 2009). A reasonable interpretation is therefore that northwestward displacement of the eugeoclinal allochthon overlying the El Shalul pluton was over by *c.* 600 Ma.

7. Conclusions

The El Shalul granite is a *c.* 634 Ma syn-orogenic intrusion comparable in age and geochemical signature to the Um Ba'anib orthogneiss in the core of the Meatiq Gneiss Dome. The El Shalul granite is LREE enriched and has a distinct negative Eu anomaly, typical of high-K calc-alkaline granites and indicative of plagioclase fractionation. Major and trace element data indicate derivation of the melt in a within-plate tectonic setting. A mean positive ε_{Nd} value of +7.1 indicates derivation from a juvenile Neoproterozoic crustal protolith. Nd model age calculations indicate an age of *c.* 700 Ma. LA-ICP-MS Hf-isotope data on zircons from the El Shalul granite are positive (+9.2) and support the interpretation of a juvenile Neoproterozoic crustal source rock. Hf model age calculations indicate that the protolith for the granite cannot have resided in the crust for more than 200 Ma before the melts were generated. Northwestward displacement of the eugeoclinal allochthon overlying the El Shalul granite had ceased 600 Ma before present.

Acknowledgements. We thank Jarkko Lamminen and Siri Simonsen, University of Oslo, for help with the LA-ICP-MS analyses. We also thank A. M. Lundmark for reading through and making improvements to an early draft of the manuscript. Tom Andersen is thanked for developing the software transferring the raw LA-ICP-MS data into meaningful ages and isotope ratios. Financial support for this study comes from UoO grant 'Småforsk' to Arild Andresen and NSF grant EAR-0804749 to Robert J. Stern. This is UTD geosciences contribution #1206 and a JEBEL contribution.

References

ABDEEN, M. M. & GREILING, R. O. 2005. A quantitative structural study of Late Pan-African compressional deformation in the Central Eastern Desert (Egypt) during Gondwana assembly. *Gondwana Research* **8**, 457–71.

ABDELSALAM, M. G., LIÉGEOIS, J. P. & STERN, R. J. 2002. The Sahara metacraton. *Journal of African Earth Sciences* **34**, 109–17.

AKAAD, M. K. & NOWEIR, A. 1980. Geology and lithostratigraphy of the Arabian Desert orogenic belt of Egypt between Lat. 25° 35′ and 26° 30′. *Institute of Applied Geology, King Abdul Aziz University, Jeddah Bulletin* **3**(4), 127–35.

ALI, K. A., STERN, R. J., MANTON, W. I., KIMURA, J.-I. & KHAMEES, H. A. 2009. Geochemistry, Nd isotopes and U-Pb SHRIMP zircon dating of Neoproterozoic volcanic rocks from the Central Eastern Desert of Egypt: new insights into the ∼750 Ma crust-forming event. *Precambrian Research* **171**, 1–22.

ANDERSEN, T., ANDERSSON, U. B., GRAHAM, S., ÅBERG, G. & SIMONSEN, S. L. 2009. Granitic magmatism by melting of juvenile continental crust: new constraints on the source of Paleoproterozoic granitoids in Fennoscandia from Hf isotopes in zircon. *Journal of the Geological Society, London* **166**, 233–47.

ANDERSEN, T., GRIFFIN, W. L. & PEARSON, N. J. 2002. Crustal evolution in the SW part of the Baltic Shield: the Hf isotope evidence. *Journal of Petrology* **43**, 1725–47.

ANDRESEN, A., AUGLAND, L. E., BOGHDADY, G. Y., LUNDMARK, A. M., ELNADY, O. M., HASSAN, M. A. & ABU EL-RUS, M. A. 2010. Structural constraints on the evolution of the Meatiq Gneiss Dome (Egypt), East-African Orogen. *Journal of African Earth Sciences* **57**, 413–22.

ANDRESEN, A., EL-RUS, M. A. A., MYHRE, P. I. & BOGHDADY, G. Y. 2009. U-Pb TIMS age constraints on the evolution of the Neoproterozoic Meatiq Gneiss Dome, Eastern Desert, Egypt. *International Journal of Earth Sciences* **98**, 481–97.

AUGLAND, L. E., ANDRESEN, A. & BOGHDADY, G. Y. 2011. U–Pb ID-TIMS dating of igneous and metaigneous rocks from the El-Sibai area: time constraints on the tectonic evolution of the Central Eastern Desert, Egypt. *International Journal of Earth Sciences*, published online 27 March 2011. doi.10.1007/s00053-011-0653-3.

BLICHERT-TOFT, J. & ALBARÈDE, F. 1997. The Lu-Hf geochemistry of chondrites and the evolution of the mantle-crust system. *Earth and Planetary Science Letters* **148**, 243–58.

BREGAR, M., BAUERNHOFER, A., PELZ, K., KLOETZLI, U., FRITZ, H. & NEUMAYR, P. 2002. A late Neoproterozoic magmatic core complex in the Eastern Desert of Egypt: emplacement of granitoids in a wrench-tectonic setting. *Precambrian Research* **118**, 59–82.

BREITKREUZ, C., ELIWA, H., KHALAF, I., EL GAMEEL, K., BUHLER, B., SERGEEV, S., LARIONIV, S. & MURATA, M. 2010. Neoproterozoic SHRIMP U-Pb zircon ages of silica-rich Dokhan Volcanics in the North Eastern Desert, Egypt. *Precambrian Research* **182**, 163–74.

CORFU, F., HANCHAR, J. M., HOSKIN, P. W. O. & KINNY, P. 2003. Atlas of zircon textures. In *Zircon* (eds J. M. Hanchar & P. W. O. Hoskin), pp. 469–500. Reviews in Mineralogy and Geochemistry vol. 53.

DEPAOLO, D. J. 1981. Neodymium isotopes in the Colorado Front Range and crust-mantle evolution in the Proterozoic. *Nature* **291**, 193–6.

DEPAOLO, D. J. 1983. The mean life of continents: estimates of continental recycling rates from Nd and Hf isotopic data and implications for mantle structure. *Geophysical Research Letters* **10**, 705–8.

DICKIN, A. P. 2005. *Radiogenic Isotope Geology*. Cambridge: Cambridge University Press, 492 pp.

EL-GABY, S., EL-NADY, O. & KHUDEIR, A. A. 1984 .Tectonic evolution of the basement complex in the Central Eastern Desert of Egypt. *Geologische Rundschau* **73**, 1019–36.

EL-GABY, S., LIST, F. K. & TEHRANI, R. 1988. Geology, evolution and metallogenesis of the Pan-African Belt in Egypt. In *The Pan-African Belt of Northeast Africa and Adjacent Areas* (eds S. El-Gaby & R. O. Greiling), pp. 17–68. Wiesbaden, Germany: Vieweg & Sohn.

EL-GABY, S., LIST, F. K. & TEHRANI, R. 1990. The basement complex of the Eastern Desert and Sinai. In *The Geology of Egypt* (ed. R. Said), pp. 175–84. Rotterdam: Balkema.

EL-RAMLY, M. F., GREILING, R. O., KRÖNER, A. & RASHWAN, A. A. 1984. On the tectonic evolution of the Wadi Hafafit area and environs, Eastern Desert of Egypt. *Faculty of Science, King Abdul Aziz University, Jeddah Bulletin* **6**, 113–26.

GOLDSTEIN, S. L., O'NIONS, R. K., KEITH, R. & HAMILTON, P. J. 1984. A Sm-Nd isotopic study of atmospheric dust and particulates from major river systems. *Earth and Planetary Science Letters* **70**, 221–36.

GREENBERG, J. K. 1981. Characteristics and origin of Egyptian younger granites. *Geological Society of America Bulletin* **92**, 748–840.

GREILING, R. O., ABDEEN, M. M., DARDIR, A. A., EL AKHAL, H., EL RAMLY, M. F., KAMAL EL DIN, G. M., OSMAN, A. F., RASHWAN, A. A., RICE, A. H. N. & SADEK, M. F. 1994. A structural synthesis of the Proterozoic Arabian-Nubian Shield in Egypt. *Geologische Rundschau* **83**, 484–501.

GREILING, R. O., KRÖNER, A. & EL-RAMLY, M. F. 1984. Structural interference patterns and their origin in the Pan-African basement of the southeastern Desert of Egypt. In *Precambrian Tectonics Illustrated* (eds A. Kröner & R. O. Greiling), pp. 401–12. Stuttgart, Germany: Schweitzerbart'sche Verlagsbuchhandlung.

GREILING, R. O., KRÖNER, A., EL-RAMLY, M. F. & RASHWAN, A. A. 1988. Structural relationship between the southern and central parts of the Eastern desert of Egypt: details of a fold and thrust belt. In *The Pan-African Belt of Northeast Africa and Adjacent Areas* (eds S. El-Gaby & R. O. Greiling), pp. 121–46. Weisbaden, Germany: Vieweg & Sohn.

GRIFFIN, W. L., PEARSON, N. J., BELOUSOVA, E., JACKSON, S. E., VAN ACHTERBERGH, E., O'REILLY, S. Y. & SHEE, S. R. 2000. The Hf isotope composition of cratonic mantle: LAM-MC-ICPMS analysis of zircon megacrysts in kimberlites. *Geochimica et Cosmochimica Acta* **64**, 133–47.

GRIFFIN, W. L., WANG, X., JACKSON, S. E., PEARSON, N. J., O'REILLY, S. Y., XU, X. & ZHOU, X. 2002. Zircons chemistry and magma genesis in SE China: *in situ* analysis of Hf isotopes, Pingtan and Tonglu igneous complexes. *Lithos* **61**, 237–69.

HAMIMI, Z., EL AMAWY, M. A. & WETAIT, M. 1994. Geology and structural evolution of El Shalul Dome and environs, Central Eastern Desert, Egypt. *Egyptian Journal of Geology* **38–2**, 575–959.

HARGROVE, U. S., STERN, R. J., KIMURA, J.-L., MANTON, W. I. & JOHNSON, P. R. 2006. How juvenile is the Arabian-Nubian Shield? Evidence from Nd isotopes and pre-Neoproterozoic inherited zircons in the Bi'r Umq suture zone, Saudi Arabia. *Earth and Planetary Science Letters* **252**, 308–26.

HEINONEN, A. P., ANDERSEN, T. & RËMÖ, O. T. 2010. Re-evaluation of rapakivi petrogenesis: source constraints from Hf isotope composition and zircon in the rapakivi granites and associated mafic rocks of southern Finland. *Journal of Petrology* **51**, 1687–709.

IRVINE, T. N. & BARAGAR, W. R. A. 1971. Guide to chemical classification of common volcanic rocks. *Canadian Journal of Earth Sciences* **8**, 523–48.

KHUDEIR, A. A., ABU EL-RUS, M. A., EL-GABY, S., EL-NADY, O. & BISHARA, W.W. 2008. Sr-Nd isotopes and geochemistry of the infrastructural rocks in the Meatiq and Hafafit core complexes, Eastern Desert, Egypt: evidence for involvement of pre-Neoproterozoic crust in the growth of Arabian-Nubian shield. *Island Arc* **17**, 90–108.

KHUDEIR, A. A., EL GABY, S., KAMAL EL-DIN, G. M., ASRAN, A. A. M. H. & GREILING, R. O. 1995. The pre-Pan African deformed granite cycle of the Gabal El-Sibai swell, Eastern Desert, Egypt. *Journal of African Earth Sciences* **21**, 395–406.

KRÖNER, A., GREILING, R., REISCHMANN, T., HUSSEIN, I. M., STERN, R. J., DÜRR, S., KRÜGER, J. & ZIMMER, M. 1987. Pan-African crustal evolution in the Nubian segment of Northeast Africa. In *Proterozoic Lithospheric Evolution* (ed. A. Kröner), pp. 235–57. American Geophysical Union, Geodynamics Series vol. 17.

KRÖNER, A., KRÜGER, J. & RASHWAN, A. A. A. 1994. Age and tectonic setting of granitoid gneisses in the Eastern Desert of Egypt and southwest Sinai. *Geologische Rundschau* **83**, 502–13.

KÜSTER, D., LIÉGEOIS, J.-P., MATUKOV, D., SERGEEV, S. & LUCASSEN, F. 2008. Zircon geochronology and Sr, Nd, Pb isotope geochemistry of granitoids from Bayuad Desert and Sabaloka (Sudan): evidence for a Bayudian event (920–900 Ma) preceding the Pan-African orogenic cycle (860–590 Ma) at the eastern boundary of the Saharan Metacraton. *Precambrian Research* **164**, 16–39.

LE MAITRE, R. W., BATEMAN, P., DUDEK, A., KELLER, J., LAMEYRE, J., LE BAS, M. J., SABINE, P. A., SCHMIDT, R., SORENSEN, H., STRECKEISEN, A., WOOLEY, A. R. & ZANETTI, B. 1989. *A Classification of Igneous Rocks and Glossary of Terms*. Oxford: Blackwell, 193 pp.

LIÉGEOIS, J. P. & STERN, R. J. 2010. Sr-Nd isotopes and the geochemistry of granite-gneiss complexes from the Meatiq and Hafafit domes, Eastern Desert, Egypt: no evidence for pre-Neoproterozoic crust. *Journal of African Earth Sciences* **57**, 31–40.

LUDWIG, K. R. 1998. On the treatment of concordant uranium–lead ages. *Geochimica et Cosmochimica Acta* **62**, 665–76.

LUDWIG, K. R. 2003. *User's Handbook for Isoplot 3.00: A geochronological toolkit for Microsoft Excel.* Berkeley Geochronology Center Special Publication no. 4, 70 pp.

LUGMAIR, G. W. & MARTI, K. 1978. Lunar initial ^{143}Nd/^{144}Nd: differential evolution of the lunar crust and mantle. *Earth and Planetary Science Letters* **39**, 349–57.

LUNDMARK, A. M., ANDRESEN, A., AUGLAND, L. E. & ANDERSEN, T. 2009. The Neoproterozoic East African Orogen viewed from the Eastern Desert, Egypt: an ID-TIMS age and in situ LA-ICPMS Hf isotopic study. In *NGF Abstracts and Proceedings of the Norwegian Geological Society 2009*, vol. 1 (ed. H. A. Nakrem), p. 67. Trondheim: Norsk Geologisk Forening.

LUNDMARK, A. M., ANDRESEN, A., HASSAN, M. A., AUGLAND, L. E., ABU EL-RUS, M. A. & BOGHDADY, G. Y. 2011. Repeated magmatic pulses in the East African Orogen of Central Eastern Desert, Egypt: an old idea supported by new evidence. *Gondwana Research*, published online 1 October 2011. doi.10.1016/j.gr.2011.08.017.

MOGHAZI, A. M. 2002. Petrology and geochemistry of Pan-African granitoids, Kab Amiri area, Egypt – implications for tectonomagmatic stages in the Nubian Shield evolution. *Mineralogy and Petrology* **75**, 41–67.

MOUSSA, E. M. M., STERN, R. J., MANTON, E. I. & ALI, K. A. 2008. SHRIMP zircon dating and Sm/Nd isotopic investigations of Neoproterozoic granitoids, Eastern Desert Egypt. *Precambrian Research* **160**, 341–56.

NAKAMURA, N. 1974. Determination of REE, Ba, Fe, Mg, Na and K in carbonaceous and ordinary chondrites. *Geochimica et Cosmochimica Acta* **38**, 757–75.

NELSON, B. K. & DEPAOLO, D. J. 1985. Rapid production of continental crust 1.7 to 1.9 b.y. ago: Nd isotopic evidence from the basement of the North American midcontinent. *Geological Society of America Bulletin* **96**, 746–54.

OSMAN, A. F. 1996. Structural, geological and geochemical studies of the Pan-African basement rocks, Wadi Zeidun Area, Central Eastern Desert, Egypt. *Scientific Series of the International Bureau/Forschungsztrum Julich GmbH* **39**, 262 pp.

PEARCE, J. A., HARRIS, N. B. W. & TINDLE, A. G. 1984. Trace element discrimination diagrams for the tectonic interpretation of granitic rocks. *Journal of Petrology* **25**, 956–83.

PEASE, V., SHALABY, E., AXELSSON, E., WHITEHOUSE, M. H. & OM, M. J. 2010. Neoproterozoic Wadi Nabi intrusive complex, Central Eastern Desert. *Saudi Geological Survey, Technical Report SGS-TR-2010-2*, 56–60.

PECCERILLO, R. & TAYLOR, S. R. 1976. Geochemistry of Eocene calc-alkaline volcanic rocks from Kastamonu area, northern Turkey. *Contributions to Mineralogy and Petrology* **58**, 63–81.

RAGAB, A. I., EL KALIOUBI, B. & EL ALFY, Z. 1983. Petrotectonic assemblages and crustal evolution of the area north of Abu El Tiyur, Central Eastern Desert, Egypt. *Middle East Research Center, Ain Sham University, Earth Science Series* **7**, 16.

RIES, A. C., SHACKELTON, R. M., GRAHAM, R. H. & FITCHES, W. R. 1983. Pan-African structure, ophiolites and melanges in the Eastern Desert of Egypt: a traverse at 26°N. *Journal of the Geological Society, London* **140**, 75–95.

ROSA, D. R. N., FINCH, A. A., ANDERSEN, T. & INVERNO, C. M. C. 2009. U–Pb geochronology and Hf isotope ratios of magmatic zircons from the Iberian Pyrite Belt. *Mineralogy and Petrology* **95**, 47–69.

SØDERLUND, U., PATCHETT, P. J., VERVOORT, J. D. & ISACHSEN, C. E. 2004. The ^{176}Lu decay constant determined by Lu-Hf and U-Pb isotope systematics of Precambrian mafic intrusions. *Earth and Planetary Science Letters* **219**, 311–24.

STACEY, J. S. & AGAR, R. A. 1985. U-Pb isotopic evidence for the accretion of a continental micro plate in the Zalm region of the Saudi Arabian Shield. *Journal of the Geological Society, London* **142**, 1189–203.

STERN, R. J. 1994. Arc assembly and continental collision in the Neoproterozoic East Africa Orogen: implications for the consolidation of Gondwanaland. *Annual Reviews of Earth and Planetary Science* **22**, 319–51.

STERN, R. J. 2002. Crustal evolution in the East African Orogen: a neodymium isotopic perspective. *Journal of African Earth Sciences* **34**, 309–117.

STERN, R., AVIGAD, D., MILLER, N. R. & BEYTH, M. 2006. Evidence for the Snowball Earth Hypothesis in the

Arabian-Nubian Shield and the East African Orogen. *Journal of African Earth Sciences* **44**, 1–20.
STERN, R. J., GOTTFRIED, D. & HEDGE, C. E. 1984. Late Precambrian rifting and crustal evolution in the Northeastern Desert of Egypt. *Geology* **12**, 168–71.
STERN, R. J. & HEDGE, C. E. 1985. Geochronological constraints on late Precambrian crustal evolution in the Eastern Desert of Egypt. *American Journal of Science* **285**, 97–127.
STOESER, D. & FROST, C. 2006. Nd, Pb, Sr, and O isotopic characterization of Saudi Arabian Shield terranes. *Chemical Geology* **226**, 163–88.
SULTAN, M., TUCKER, R. D., EL ALFY, Z., ATTIA, R. & RAGAB, A. G. 1994. U-Pb (zircon) ages from the gneissic terrane west of the Nile southern Egypt. *Geologische Rundschau* **83**, 514–22.
VERVOORT, J. & BLICHERT-TOFT, J. 1999. Evolution of the depleted mantle: Hf isotope evidence from juvenile rocks through time. *Geochimica et Cosmochimica Acta* **63**, 533–56.
WHALEN, J. B., CURRIE, K. L. & CHAPELL, B. W. 1987. A-type granites: geochemical characteristics, discrimination and petrogenesis. *Contributions to Mineralogy and Petrology* **95**, 407–19.
WHITEHOUSE, M. J., STOESER, D. B. & STACEY, J. S. 2001*a*. The Khida Terrane – geochronological and isotopic evidence for Paleoproterozoic and Archean crust in the Eastern Arabian shield. *Gondwana Research* **4**, 200–2.
WHITEHOUSE, M. J., WINDLEY, B. F., BA-TATT, M. A., FANNING, C. M. & REX, D. C. 1998. Crustal evolution and terrane correlation in the eastern Arabian Shield, Yemen: geochronological constraints. *Journal of the Geological Society, London* **155**, 281–95.
WHITEHOUSE, M. J., WINDLEY, B. F., STOESER, D. B., AL-KHIRBASH, S., BA-BTTAT, M. A. O. & HAIDER, A. 2001*b*. Precambrian basement character of Yemen and correlations with Saudi Arabia and Somalia. *Precambrian Research* **105**, 357–69.
WILDE, S. A. & YOUSSEF, K. 2000. Significance of SHRIMP U-Pb dating of the Imperial Porphyry and associated Dokhan Volcanics, Gabal Dokhan, North Eastern Desert, Egypt. *Journal of African Earth Sciences* **31**, 403–13.
WILDE, S. A. & YOUSSEF, K. 2002. A re-evaluation of the origin and setting of the Late Precambrian Hammamat Group based on SHRIMP U-Pb dating of detrital zircons from Gebel Umm Tawat, North Eastern Desert, Egypt. *Journal of the Geological Society, London* **159**, 595–604.